Vertically Aligned Carbon Nanotubes Grown by Pyrolysis of Iron, Cobalt, and Nickel Phthalocyanines

Nam Seo Kim, Yun Tack Lee, and Jeunghee Park*
Department of Chemistry, Korea University, Jochiwon 339-700, South Korea

Jae Bum Han and Young Sang Choi
Department of Chemistry, Korea University, Anam 1 Seoul 136-701, South Korea

Seung Yeol Choi and Jaebum Choo
Department of Chemistry, Hanyang University, Ansan 425-791, South Korea

Gang Ho Lee
Department of Chemistry, Kyungpook National University, Taegu 702-701, South Korea

Received: April 4, 2003; In Final Form: June 12, 2003

Carbon nanotubes (CNTs) were grown vertically aligned on silicon oxide substrates by pyrolyzing iron phthalocyanine (FePc), cobalt phthalocyanine (CoPc), and nickel phthalocyanine (NiPc) in the temperature range 700−1000 °C. As the temperature increases from 700 to 1000 °C, the growth rate of CNTs increases by a factor of approximately 45 and the average diameter increases from 30 to 80 nm. The CNTs grown using FePc exhibit about 2 times higher growth rate than those using CoPc and NiPc. The CNTs usually have a cylindrical structure, and a bamboo-like structure with a larger diameter at the higher temperature. The CNTs are doped with 2−6 at. % nitrogen atoms. The nitrogen content tends to decrease with the temperature increase. The CNTs grown using NiPc contain a higher nitrogen concentration compared to those grown using FePc and CoPc. The degree of crystalline perfection of the graphitic sheets increases with the temperature, but depends on the catalyst and the nitrogen content. The Arrhenius plot provides the activation energy 30 ± 3 kcal/mol for all three sources, which is similar to the diffusion energy of carbon in bulk metal. This suggests that the bulk diffusion of carbon plays a decisive role in the growth of CNTs. The strain for the joint between the compartment layer and the wall determines the structure of the CNTs.

1. Introduction

Carbon nanotubes (CNTs) are currently attractive materials for a diverse range of applications because of their extraordinary mechanical and electrical properties.[1,2] Important potential applications include field emission displays (FED)[3,4] and nanoscale electronic devices.[5−8] For some applications, e.g., FED, it is highly desirable to prepare aligned CNTs so that their properties can be easily evaluated and they can be incorporated effectively into devices.[9] Various methods, e.g., arc discharge,[10,11] laser ablation,[12] pyrolysis,[13] and chemical vapor deposition (CVD),[9,14] have been developed for the production of CNTs. Among those methods, aligned CNTs on the substrates could be usually achieved by the pyrolysis of organometallic compounds or CVD of hydrocarbons over prelocated catalysts on substrate.

The pyrolysis of iron phthalocyanine ($FeC_{32}N_8H_{16}$, designated as FePc hereafter), cobalt phthalocyanine (CoPc), and nickel phthalocyanine (NiPc) was found to be a simple and efficient method, since those molecules contain both the catalyst and carbon source required for the nanotube growth.[15−33] The evaporated phthalocyanine molecules are pyrolyzed to generate the metal atoms or clusters deposited on the substrate. This leads to the formation of Fe (or Co, Ni) nanoparticles that are known as effective catalysts for the growth of CNTs. Despite tremendous works, a direct comparison for the use of FePc, CoPc, and NiPc has not been focused yet. Such a comparison would reveal the role of catalyst in the growth of CNTs and help to elucidate the growth mechanism.

In the present work, we have investigated the growth properties of vertically aligned CNTs depending on the pyrolysis source and temperature. The CNTs were grown on silicon oxide substrate via the pyrolysis of FePc, NiPc, and CoPc under argon (Ar)/hydrogen (H_2) flow over the temperature range 700−1000 °C. Configuration and structural characteristics of CNTs were examined using scanning electron microscopy (SEM), transmission electron microscopy (TEM), and Raman spectroscopy. The growth rate and the crystallinity of graphitic sheets for the CNTs grown using three phthalocyanine molecules have been assessed to understand the catalytic activity in the growth process.

2. Experimental Section

FePc (97+%, Aldrich), CoPc (97+%, Aldrich), and NiPc (97+%, Aldrich) were used without further purification. Silicon substrate (1 cm × 3 cm) was thermally oxidized to form 300 nm thick oxide layers. A pyrolysis reactor (inner diameter of the quartz tube 25 mm and effective heating length 55 cm) was heated in a dual furnace fitted with independent temperature controllers. About 0.1−0.2 g of FePc (or CoPc, NiPc) and the silicon oxide substrate was placed in the first and second heating stages, respectively. The mixture was vaporized at 550 °C and carried by the flow of Ar (30−150 sccm)/H_2 (5−10 sccm) into the second heating stage of the quartz tube, where the pyrolysis was performed at 700−1000 °C. The CNTs were grown for 20

* Corresponding author. E-mail: parkjh@korea.ac.kr.

10.1021/jp034895o CCC: $25.00
Published on Web 07/25/2003

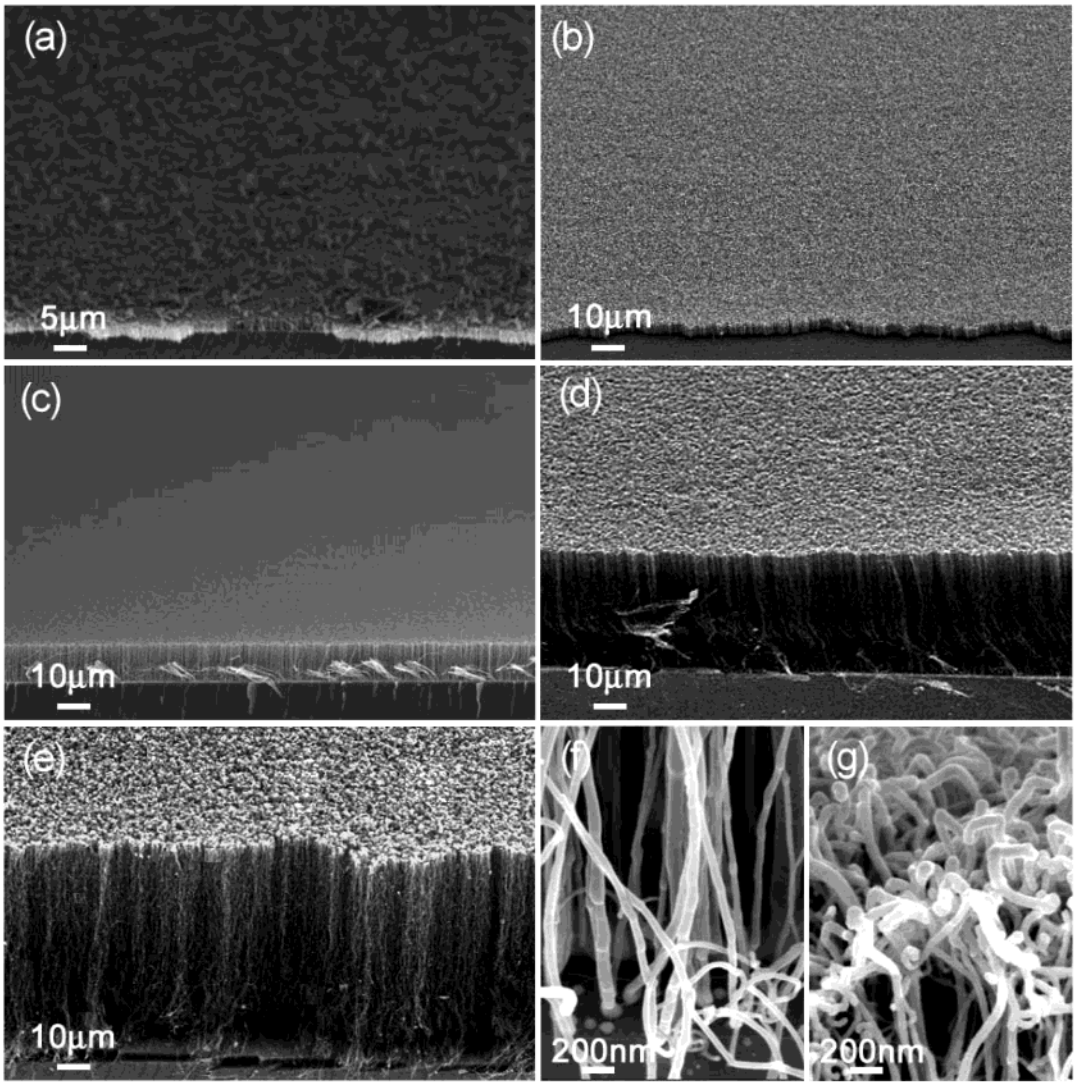

Figure 1. SEM micrographs of the vertically aligned CNTs grown on silicon oxide substrates, by pyrolysis of FePc at (a) 700, (b) 750, (c) 800, (d) 900, and (e) 1000 °C. Magnified image reveals (f) the root and (g) the closed tip of the CNTs.

min. The reactor was cooled to room temperature under ambient Ar after the growth. The CNTs grown on the substrates were analyzed by employing SEM (Hitachi S-4300), TEM (Hitachi H9000-NAR, 300 kV), and Raman spectroscopy (Renishaw Micro-Raman 2000) using the 514.5 nm line of argon ion laser. The composition of nanotubes was determined using Auger spectroscopy (Physical Electronics PHI 680) or X-ray photoelectron spectroscopy (PHI 5800).

3. Results

(1) Morphology and Growth Rate of CNTs. SEM images of the vertically aligned CNTs on the substrates are displayed in Figure 1. High-purity CNTs are grown at 700, 750, 800, 900, and 1000 °C using FePc (Figures 1a−e). The density of CNTs is higher than $10^{10}/cm^2$. The respective lengths are 2.5, 5, 15, 35, and 70 μm. From the several experimental runs, it is found that the average length of CNTs grown using FePc is 1.5 ± 1, 3 ± 2, 15 ± 5, 35 ± 10, and 70 ± 20 μm at 700, 750, 800, 900, and 1000 °C, respectively. These CNTs are grown on top of the catalytic particles deposited on the substrate (Figure 1f). The diameter of CNTs is smaller than the size of nanoparticles. The tip is closed without any capped nanoparticles (Figure 1g). Energy-dispersive X-ray spectroscopy on the tip part reveals a negligible amount of Fe element.

Parts a, b, and c of Figure 2 show the CNTs grown using CoPc at 800, 900, and 1000 °C, respectively. The respective lengths are 8, 13, and 40 μm. Parts d, e, and f of Figure 2 show lengths of 7, 27, and 50 μm for the CNTs grown using NiPc, respectively, at 850, 950, and 1000 °C. Using CoPc and NiPc, we could not succeed in synthesizing the CNTs at temperatures below 800 °C. The average length as a function of temperature is summarized in Table 1.

Dividing the length by the growth time (20 min) yields the average growth rate of CNTs in units of micrometers per minute. As the temperature increases from 700 to 1000 °C, the growth rate enhances nonlinearly by a factor of 45 for the CNTs grown using FePc. The growth rate of CNTs grown using FePc is about 2 times higher than the case of CoPc and NiPc. The growth rate as a function of temperature is plotted in Figure 3, showing a nonlinear increase of the growth rate. The growth rate of CNTs was obtained within the time regime that the constant growth rate is maintained. The growth rate is constant during 30 min, but after that the growth rate decreases as the carbonaceous particles cover the surface of substrate. The value of the growth rate is reliable within experimental error, since the experiments were carried out many times to derive accurate numbers.

(2) Structure of CNTs. We obtained TEM images for the CNTs grown from the pyrolysis of FePc, CoPc, and NiPc. The

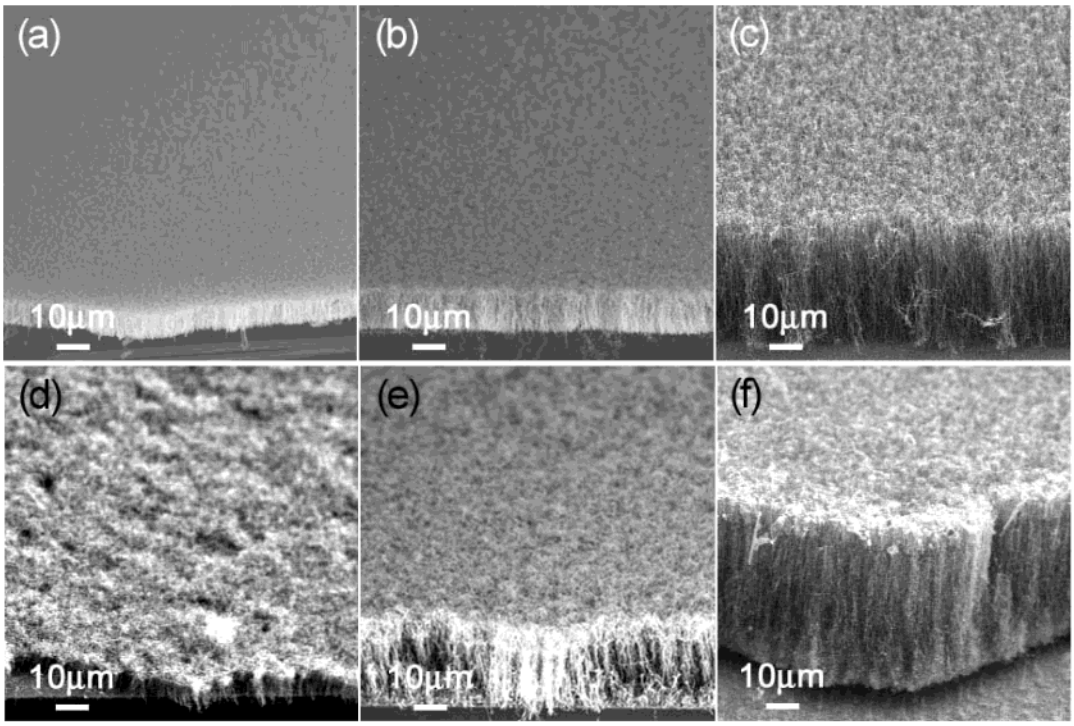

Figure 2. SEM micrographs of vertically aligned CNTs grown on silicon oxide substrates, by pyrolysis of (a) CoPc at 800 °C, (b) CoPc at 900 °C, (c) CoPc at 1000 °C, (e) NiPc at 850 °C, (f) NiPc at 950 °C, and (g) NiPc at 1000 °C.

TABLE 1: Growth Rate, Average Diameter, Nitrogen Content, and Degree of Crystallinity of CNTs Grown via Pyrolysis of FePc, CoPc, and NiPc at Various Temperatures

source	temp (°C)	av length (μm)	growth rate (μm/min)	diam range (nm)	av diam (nm)	nitrogen concen[a] (%)	I_D/I_G[b]
FePc	700	1.5 ± 1	0.075 ± 0.05	10−15	10	3.9	0.87
	750	3 ± 2	0.15 ± 0.1	10−30	20	3.5	0.72
	800	15 ± 5	0.75 ± 0.25	15−35	25	3.2	0.70
	900	35 ± 10	1.8 ± 0.5	20−60	40	2.6	0.62
	1000	70 ± 20	3.5 ± 1	50−110	80	1.6	0.55
CoPc	800	8 ± 2	0.4 ± 0.1	20−40	30	2.5	0.71
	900	12 ± 3	0.6 ± 0.2	30−80	50	2.1	0.68
	1000	35 ± 10	1.8 ± 0.5	50−110	80	1.6	0.55
NiPc	850	7 ± 2	0.4 ± 0.1	20−40	30	5.6	0.73
	900	18 ± 5	0.8 ± 0.3	30−80	50	4.8	0.70
	950	25 ± 10	1.3 ± 0.5	40−90	65	4.2	0.69
	1000	40 ± 10	1.8 ± 0.5	50−120	90	3.8	0.66

[a] Atomic %, with an error of 10%. [b] The intensity ratio of D band relative to G band, with an error of 5%.

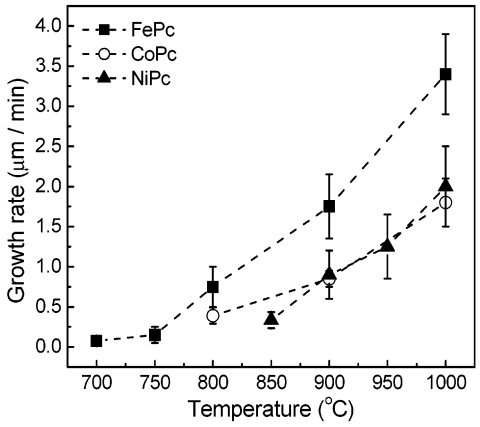

Figure 3. Growth rate vs temperature for CNTs grown via pyrolysis of FePc, CoPc, and NiPc.

CNTs were taken off the substrate by a razor and dispersed in ethanol to load homogeneously on the TEM grid. Parts a, b, c, and d of Figure 4 show the general morphology of the CNTs grown using FePc at 700, 800, 900, and 1000 °C, respectively. The diameter ranges are 10−15, 15−35, 20−60, and 50−110 nm, showing wider distribution at higher temperature. The respective average diameters of CNTs are 10, 25, 40, and 80 nm. The CNTs grown at 700 and 800 °C exhibit a cylindrical structure without any obvious compartment layers. The catalytic nanoparticles are frequently encapsulated inside the nanotubes. At temperatures higher than 900 °C, a number of CNTs exhibit a bamboo-like structure when the diameter is larger than about 50 nm. The average diameters of the CNTs at various temperatures are listed in Table 1.

Parts e and f of Figure 4 show CNTs grown at 900 °C using CoPc and NiPc, respectively. The average diameter is 50 nm. The CNTs have the same average diameter for FePc, CoPc, and NiPc at a given temperature. The CNTs grown using CoPc show the same structural feature as those grown using FePc. In contrast, most of the CNTs grown using NiPc exhibit the bamboo-like structure irrespective of the diameter, for all growth temperatures. The nanotubes usually have a closed tip and often encapsulate the catalytic particles (Figure 4g). The roots are

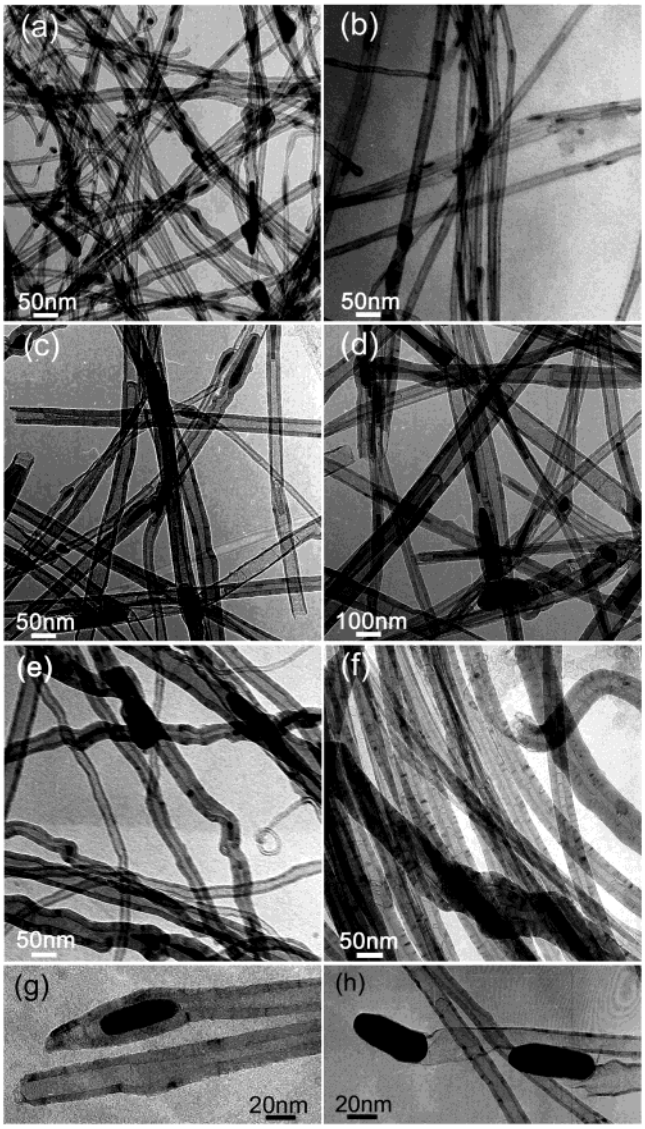

Figure 4. TEM image for bamboo-like structured CNTs grown via pyrolysis of (a) FePc at 700 °C, (b) FePc at 800 °C, (c) FePc at 900 °C, (d) FePc at 1000 °C, (e) CoPc at 900 °C, and (f) NiPc at 900 °C. The average diameter increases with the growth temperature. The CNTs have (g) the closed tip and (h) the root capped with the catalytic particles.

frequently open, separated from the catalytic particle. They are sometimes capped with the catalytic particles (Figure 4h).

(3) Crystallinity of the Graphitic Sheets. Figure 5 shows high-resolution TEM (HRTEM) images for typical CNTs grown using FePc at 800, 900, and 1000 °C, and whose diameter is smaller than 50 nm. The graphitic sheets are aligned parallel to the tube axis. The graphitic sheets of the CNT grown at 800 °C are waved over a short range (Figure 5a). The CNT grown at 900 °C exhibits a higher degree of crystalline perfection than that at 800 °C (Figure 5b). At 1000 °C the graphitic sheets are in a highly ordered crystalline structure (Figure 5c). The degree of crystalline perfection increases progressively with temperature. The outer graphitic sheets are usually less crystalline than the inner graphitic sheets. The insets show the magnified view for the right side of the wall. The graphitic sheets are separated by ~0.34 nm.

For the CNTs grown using CoPc and NiPc, the HRTEM images reveal the enhanced ordering of graphitic sheets with temperature. It is found that the CNTs grown using FePc usually exhibit a higher degree of crystalline perfection than those grown using CoPc and NiPc at a given temperature. The bamboo-like nanotubes grown using NiPc are in the worst crystalline structure among those grown using the three phthalocyanine molecules.

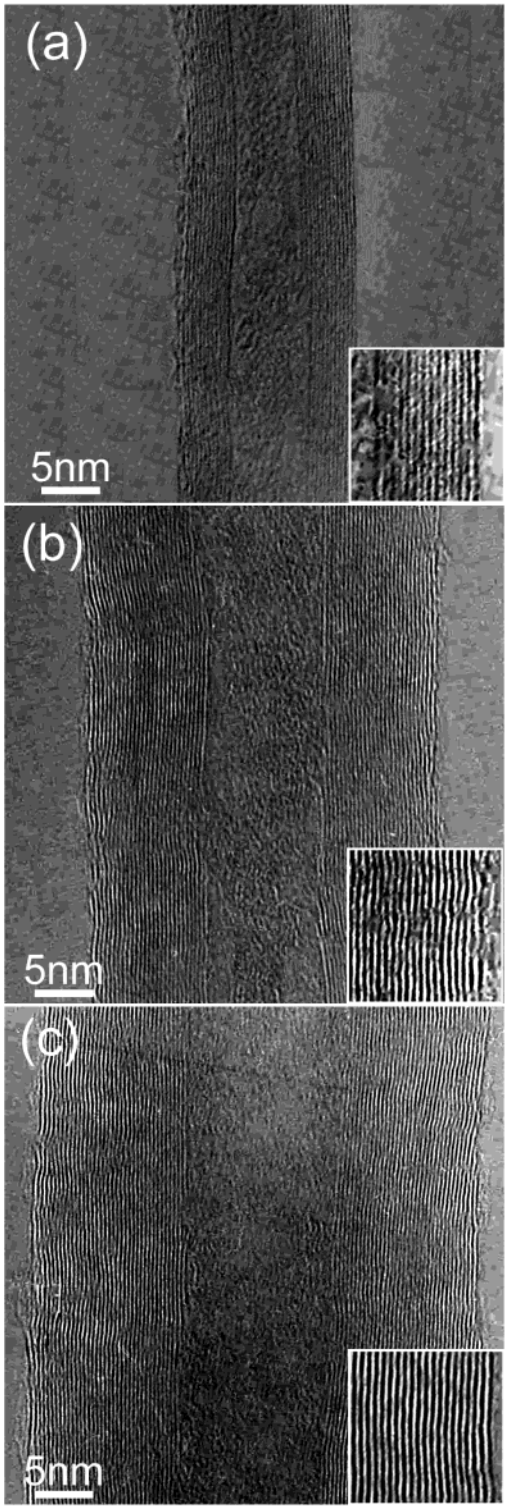

Figure 5. HRTEM images for typical CNTs grown via pyrolysis of FePc at (a) 800, (b) 900, and (c) 1000 °C. The degree of crystalline perfection increases with temperature.

To obtain the information about the crystallinity of entire CNTs, Raman spectroscopy was used. First-order Raman spectra for the CNTs grown using FePc, CoPc, and NiPc at 900 °C are displayed in Figure 6a. All spectra show mainly two Raman bands at ~1580 cm^{-1} (G band) and ~1350 cm^{-1} (D band). The G band is originated from the Raman active E_{2g} mode due

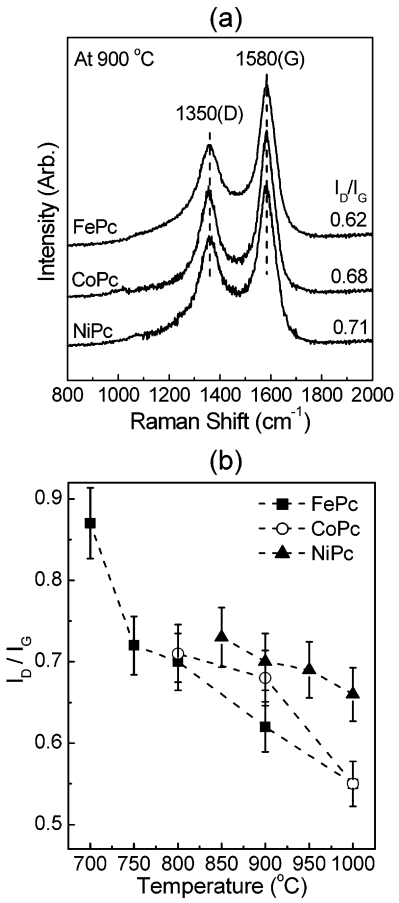

Figure 6. (a) Raman spectrum of CNTs grown via pyrolysis of FePc, CoPc, and NiPc at 900 °C. (b) Plot of I_D/I_G values vs temperature.

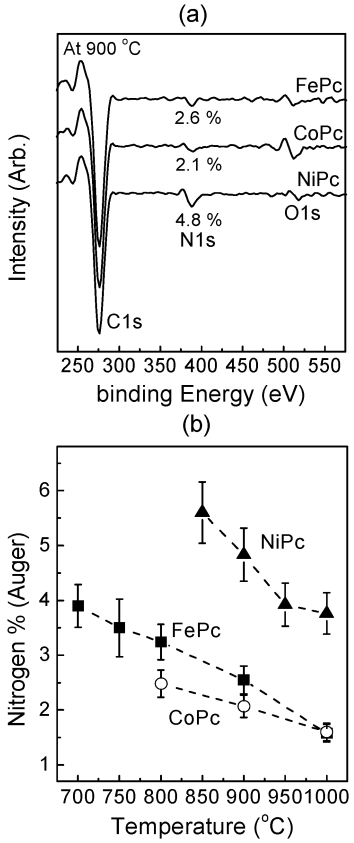

Figure 7. Auger spectra of CNTs grown using FePc, CoPc, and NiPc at 900 °C, showing N content of 2.6, 2.1, and 4.8 at. %, respectively. (b) Plot of N content for CNTs grown as a function of temperature.

to in-plane atomic displacements. The origin of D has been explained as disorder-induced features due to the finite particle size effect or lattice distortion.[34,35] It was noted that the intensity ratio of D band to G band (I_D/I_G) has a linear relation with the inverse of the in-plane crystallite dimension.[34] The values of I_D/I_G are 0.62, 0.68, and 0.70, respectively, for the CNTs grown using FePc, CoPc, and NiPc. This indicates that the degree of long-range ordered crystalline perfection would be higher for the CNTs grown using FePc compared to those grown using CoPc and NiPc. The values of I_D/I_G versus the growth temperature have been plotted in Figure 6b, showing a decrease of the I_D/I_G value with temperature increase. Over the temperature range 800−1000 °C, the best crystallinity of graphitic sheets is found from the CNTs grown using FePc. The degree of crystallinity is always lowest for the CNTs grown using NiPc.

(4) Concentration of N Atoms Doped in CNTs. Figure 7a shows the Auger spectroscopic data for the CNTs grown using FePc, CoPc, and NiPc at 900 °C. The C 1s, N 1s, and O 1s peaks appear at 275, 389, and 510 eV, respectively. A strong and sharp peak at 275 eV confirms that the major component is carbon. The O peak arises from the oxygen in air and/or adsorbed on the surface of the nanotubes. The N content (in at. %) is 2.6%, 2.1%, and 4.8%, respectively, for FePc, CoPc, and NiPc.

Figure 7b shows a plot of the N content as a function of temperature. As the temperature increases from 700 to 1000 °C, the N content decreases from 3.9% to 1.6% for FePc. The data are summarized in Table 1. The N content reaches 5.6% when NiPc is pyrolyzed at 850 °C. The CNTs grown using NiPc are more highly doped with N atoms than those grown using FePc and CoPc at a given temperature.

4. Discussion

Vertically aligned CNTs usually grow under a restricted growth condition that the metal particles are formed on the substrates with nanometer size and density as high as 10^{10}/cm^2. At higher temperature, the average size of catalytic nanoparticles increases and the distribution becomes broader due to the more efficient agglomeration of the nanoparticles. The present CNTs have a root on the catalytic particles deposited on the substrate and a closed tip without the capped catalytic particles, implying that they are probably grown from the catalytic particles deposited on the substrate. The growth mechanism would correspond to a typical base growth mechanism, which agrees with the work of other groups.[19,27]

We previously investigated the growth rate of CNTs on Fe, Co, and Ni nanoparticles deposited on alumina substrates by thermal CVD of acetylene (C_2H_2) in the temperature range 900−1000 °C.[36] The nanoparticles were formed using a thin film of metal salt, followed by ammonia (NH_3) pretreatment. The growth rate of CNTs on the Fe catalyst was about 2 times higher than those on the Co and Ni catalysts over the temperature range. The growth rate enhances by a factor of approximately 2 for the temperature increase from 900 to 1000 °C, irrespective of the catalyst. That result is remarkably consistent with the present result that the CNTs grown using FePc exhibit about 2 times higher growth rate than those using CoPc and NiPc. There is also exceptional agreement for the temperature dependence of the growth rate. Therefore, we conclude that the growth rate of CNTs grown by the pyrolysis of FePc, CoPc, and NiPc would be determined by the catalytic activity of Fe, Co, and Ni nanoparticles.

We explained properly the result of CVD by the assumption that the growth reaction of CNTs is simply a first-order

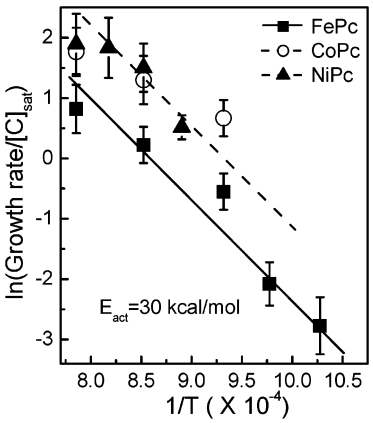

Figure 8. Arrhenius plot for growth rates of CNTs, providing activation energy (E_{act}) of 30 ± 3 kcal/mol, for FePc, CoPc, and NiPc.

diffusion-controlled reaction; the growth rate (υ) can be defined as $\upsilon = k_d$[C], where k_d is proportional to the diffusion coefficient of carbon and [C] is the saturated concentration of carbons in bulk γ-Fe, Co, and Ni. For the present result, let us infer the same assumption of the first-order diffusion-controlled reaction. The carbons are saturated into bulk γ-Fe, Co, and Ni, by an extent of 3.5−6.8, 1−1.5, and 0.7−1.5 at. % in the temperature range 700−1000 °C.[37,38] Using the known diffusion coefficient of carbon, we can estimate the relative growth rate which is consistent with the present result. Moreover, by plugging the value of saturated carbon concentration into [C] ($[C]_{sat}$), the Arrhenius plot of ln(growth rate/$[C]_{sat}$) vs $1/T$ (K) can be used to derive the activation energy as displayed in Figure 8. The data fit well to a linear function, providing the activation energy of 30 ± 3 kcal/mol. This value is close to the diffusion energy of carbon in bulk γ-Fe, Co, and Ni, which is 35, 37, and 33 kcal/mol, respectively.[39,40] Therefore, we suggest that the bulk diffusion rate of carbons is a main factor in determining the growth rate of the present CNTs. It was reported that the growth rate of carbon nanofibers or CNTs has an inverse dependence on the size of catalytic particles.[40−42] Since the size of catalytic particles limits the diameter of CNTs, the growth rate may decrease with increasing diameter of CNTs. If all CNTs were of the same diameter for all temperatures, the activation energy would be even closer to the diffusion energy of carbon.

For the bamboo-like structured CNTs grown using thermal CVD of C_2H_2, we described a base growth model on the basis that the rate-determining step is the bulk diffusion of carbon.[36,43,44] In this work, the cylindrical structured CNTs are usually grown and the bamboo-like structure is often formed when the diameter is larger than about 50 nm, following a base growth mechanism. The analysis of the growth rate suggests that the bulk diffusion of carbon can also play an important role in the growth of the cylindrical CNTs. Therefore, we present the following description for the growth of cylindrical and bamboo-like CNTs by adopting the growth model of bamboo-like CNTs.

Carbons can dissolve into the catalytic nanoparticle and diffuse via the surface and bulk. They probably form a miscible alloy with the catalytic nanoparticles. As the carbons saturate in the catalytic nanoparticle, they start to precipitate. Initially, they form graphitic sheets as a cap on the catalytic particles. As the cap lifts off the catalytic particle, a closed tip with a hollow inside is produced. The motive force departing from the catalytic particle can be the stress accumulated under the cap. Part of the catalytic nanoparticles can be split and encapsulated inside the cap due to such stress. The carbons accumulated on the surface of catalytic particle inside the tube, probably mainly via bulk diffusion, build the inner graphitic sheets of the wall as well as the compartment graphitic sheets on the catalytic particle. When the compartment layers are fully grown, the compartment layer can join with the graphitic sheets of the wall. However, if the diameter is small, they must be bent seriously and overcome a tremendous stress. Then the graphitic sheets of the wall are grown straight with negligible disturbance of the joints with compartment layers. Consequently, cylindrically structured CNTs are produced. When the diameter increases (at higher temperature), the compartment layers can join with less strain. The periodic production of the compartment layers results in the formation of the bamboo-like structure. Since the multiwalled graphitic sheets grow simultaneously, the growth rate of inner sheets can determine the growth rate of the cylindrical and bamboo-like structured CNTs.

As the temperature increases, the growth rate of CNTs increases due to the enhanced bulk diffusion rate of carbons. The increased bulk diffusion rate of carbon can supply sufficient carbons to form the less defective graphitic sheets. Therefore, the crystallinity of graphitic sheets can be correlated with the growth rate. The temperature dependence of the growth rate and the crystallinity of graphitic sheets can be thus suitably explained by the bulk diffusion of carbons.

The N atoms are inevitably generated from the dissociation of phthalocyanine molecules and dissolve into the catalytic nanoparticles. The dissolved N atoms precipitate with the carbons during the growth of CNTs, resulting in the N doping of the CNTs. Auger spectroscopic data reveal that the maximum N content in the present CNTs is about 6%, which is consistent with the result of other groups that the N content usually did not exceed 10%.[29] We were able to control the N content of CNTs grown via thermal CVD of C_2H_2 (or methane) and NH_3.[45] It was found that the growth rate of CNTs is independent of the 2−6% N doping. Therefore, the activation energy evaluated from the growth rate is valid even though the N content of the CNTs varies with the temperature.

The incorporation of the N atoms in the graphitic sheets deteriorates the crystallinity of the graphitic sheets. Pyridine-type N atoms reduce the crystalline perfection of the graphitic sheets.[46] The less crystalline graphitic sheets probably exhibit more flexibility. Then the compartment layers are smoothly bent and their connection with the wall takes place under less stress. The increase of N content facilitates the joint of the wall and compartment layers, producing the bamboo-like structure. This can explain why the highly doped CNTs grown using NiPc exhibit distinctively the bamboo-like structure.

The decrease of the N content at higher temperature contributes in enhancing the crystalline perfection of the CNTs. At a given temperature, the graphitic sheets of CNTs grown using FePc are of better crystallinity than those grown using CoPc, despite the higher N content. This is probably related to the higher diffusion rate of carbon in the Fe nanoparticles compared to the Co nanoparticles. This provides more evidence that the bulk diffusion rate of carbons plays an important role in determining the crystallinity of CNTs. However, the question is why the CNTs grown using NiPc contain the higher N concentration. A possible explanation is that the saturated concentration of N atom in bulk Ni would be much higher than that in bulk Fe. According to the available phase diagram, the N atoms can be saturated with 25 at. % in Ni and with 10 at. % in γ-Fe, at 700 °C.[37] Another question arises for the N content depending on the temperature. The saturated concentration of the N atoms in γ-Fe decreases from 10 to 8 at. % as the

temperature increases from 700 to 900 °C, which is opposite to the saturated C atoms. This would rationalize the decrease of the N content at higher temperature. However, since no further data are available, we cannot provide a definite explanation for the dependence of the N content on the temperature and the catalyst.

The synthesis of N-doped CNTs has been recently thought of as a possible method to control the electronic properties of CNTs in a well-defined way. An enhancement of conductivity is expected, because the additional electrons contributed by the N atom provide electron carriers for the conduction band.[46] The advantage of such nanotubes is that their electronic properties are primarily determined by the composition and are thus relatively easy to control. Therefore, the pyrolysis of phthalocyanine molecules would be an efficient route for the production of CNTs with a controlled N concentration.

5. Conclusion

CNTs were grown vertically aligned on silicon oxide substrates via the pyrolysis of FePc, CoPc, and NiPc in the temperature range 700−1000 °C. The growth rate of CNTs grown using FePc enhances approximately by a factor of 45 for the temperature increase from 700 to 1000 °C. Their growth rate is about 2 times higher than those using CoPc and NiPc over the temperature range 800−1000 °C. The average diameter of CNTs increases from 30 to 80 nm for the temperature increase from 700 to 1000 °C. They exhibit a cylindrical structure where the graphitic sheets are aligned parallel to the tube axis. As the temperature increases, the compartment layers appear inside the CNTs whose diameter is larger than about 50 nm. Raman spectra reveal that the crystallinity of CNTs grown using NiPc is worse than that of the CNTs grown using FePc and CoPc. Auger spectroscopy reveals that the nanotubes are doped with N atoms in a concentration of 2−6%. As the temperature increases, the N content decreases. In particular, the CNTs grown using NiPc exhibit higher N content than the other CNTs.

On the basis of the assumption that the rate-determining step of the CNT growth is a diffusion-controlled first-order reaction whose rate is proportional to the diffusion coefficient and saturated concentration of carbons in bulk metal, the Arrhenius plot provides activation energy of 30 ± 3 kcal/mol for all three catalysts. This activation energy is similar to the diffusion energy of carbon in bulk metal, suggesting that bulk diffusion plays a major role in the growth of the present CNTs. We suggest a growth model for the cylindrical and bamboo-like structured CNTs. The strain for the joint between the compartment layer and the wall determines the structure of the CNTs. At the smaller diameter, the cylindrical structure is formed due to the larger strain. The N doping reduces the degree of crystalline perfection and produces the bamboo-like structure due to a release of strain. The degree of the crystalline perfection of graphitic sheets is in a good correlation with the growth rate and the N content.

Acknowledgment. KOSEF (Project No. R04-2002-000-200088-012003) supported the present work. SEM analyses were performed at the Basic Science Research Center in Seoul.

References and Notes

(1) Treacy, M. M. J.; Ebbesen, T. W.; Gibson, J. M. *Nature* **1996**, *381*, 678.

(2) Odom, T. W.; Huang, J.-L.; Kim, P.; Lieber, C. M. *Nature* **1998**, *391*, 62.

(3) de Heer, W. A.; Châtelain, A.; Ugarte, D. *Science* **1995**, *270*, 1179.

(4) Saito, Y.; Hamaguchi, K.; Hata, K.; Uchida, K.; Tasaka, Y.; Ikazaki, F.; Yumura, M.; Kasuya, A.; Nishina, Y. *Nature* **1997**, *389*, 554.

(5) Tans, S. J.; Verschueren, A. R. M.; Dekker, C. *Nature* **1998**, *393*, 49.

(6) Rueckes, T.; Kim, K.; Joselevich, E.; Tseng, G. Y.; Cheung, C.-L.; Lieber, C. M. *Science* **2000**, *289*, 94.

(7) Bachtold, A.; Hadley, P.; Nakanishi, T.; Dekker, C. *Science* **2001**, *294*, 1317.

(8) Liang, W.; Bockrath, M.; Bozovic, D.; Hafner, J. H.; Tinkham, M.; Park, H. *Nature* **2001**, *411*, 665.

(9) Fan, S.; Chapline, M. G.; Franklin, N. R.; Tombler, T. W.; Cassell, A. M.; Dai, H. *Science* **1999**, *283*, 512.

(10) Bethune, D. S.; Kiang, C. H.; deVries, M. S.; Gorman, G.; Savoy, R.; Vazquez, J.; Beyers, R. *Nature* **1993**, *363*, 605.

(11) Journet, C.; Maser, W. K.; Bernier, P.; Loiseau, A.; Lamy de la Chapelle, M.; Lefrant, S.; Deniard, P.; Lee, R.; Fischer, J. E. *Nature* **1997**, *388*, 756.

(12) Thess, A.; Lee, R.; Nikolaev, P.; Dai, H.; Petit, P.; Robert, J.; Xu, C.; Lee, Y. H.; Kim, S. G.; Rinzler, A. G.; Colbert, D. T.; Scuseria, G. E.; Tománek, D.; Fisher, J. E.; Smalley, R. E. *Science* **1996**, *273*, 483.

(13) Terrones, M.; Grobert, N.; Olivares, J.; Zhang, J. P.; Terrones, H.; Kordatos, K.; Hsu, W. K.; Hare, J. P.; Townsend, P. D.; Prassides, K.; Cheetham, A. K.; Kroto, H. W.; Walton, D. R. M. *Nature* **1997**, *388*, 52.

(14) Ren, Z. F.; Huang, Z. P.; Xu, J. W.; Wang, J. H.; Bush, P.; Siegal, M. P.; Provencio, P. N. *Science* **1998**, *282*, 1105.

(15) Yudasaka, M.; Kikuchi, R.; Ohki, Y.; Yoshimura, S. *Carbon* **1997**, *35*, 195.

(16) Araki, H.; Kajii, H.; Yoshino, K. *Jpn. J. Appl. Phys.* **1999**, *38*, L1351.

(17) Araki, H.; Katayama, T.; Yoshino, K. *Appl. Phys. Lett.* **2001**, *79*, 2636.

(18) Katayama, T.; Araki, H.; Kajii, H.; Yoshino, K. *Synth. Met.* **2001**, *121*, 1235.

(19) Katayama, T.; Araki, H.; Yoshino, K. *J. Appl. Phys.* **2002**, *91*, 6675.

(20) Huang, S.; Dai, L.; Mau, A. W. H. *J. Phys. Chem. B* **1999**, *103*, 4223.

(21) Huang, S.; Dai, L.; Mau, A. W. H. *J. Mater. Chem.* **1999**, *9*, 1221.

(22) Huang, S.; Mau, A. W. H.; Turney, T. W.; White, P. A.; Dai, L. *J. Phys. Chem. B* **2000**, *104*, 2193.

(23) Li, D.-C.; Dai, L.; Huang, S.; Mau, A. W. H.; Wang, Z. L. *Chem. Phys. Lett.* **2000**, *316*, 349.

(24) Huang, S.; Dai, L. *J. Phys. Chem. B* **2002**, *106*, 3543.

(25) Wang, X. B.; Liu, Y. Q.; Zhu, D. B. *Appl. Phys. A* **2000**, *71*, 347.

(26) Wang, X.; Liu, Y.; Yu, G.; Xu, C.; Zhang, J.; Zhu, D. *J. Phys. Chem. B* **2001**, *105*, 9422.

(27) Wang, X.; Hu, W.; Liu, Y.; Long, C.; Xu, Y.; Zhou, S.; Zhu, D.; Dai, L. *Carbon* **2001**, *39*, 1553.

(28) Wang, X.; Liu, Y.; Zhu, D. *Chem. Commun.* **2001**, *8*, 751.

(29) Li, S.; Li, H.; Wang, X.; Song, Y.; Liu, Y.; Jiang, L.; Zhu, D. *J. Phys. Chem. B* **2002**, *106*, 9274.

(30) Wang, X.; Liu, Y.; Hu, P.; Yu, G.; Xiao, K.; Zhu, D. *Adv. Mater.* **2002**, *14*, 1557.

(31) Wang, X.; Liu, Y.; Zhu, D. *Adv. Mater.* **2002**, *14*, 165.

(32) Wang, X.; Liu, Y.; Zhu, D.; Zhang, L.; Ma, H.; Yao, N, Zhang, B. *J. Phys. Chem. B* **2002**, *106*, 2186.

(33) Suenaga, K.; Yudasaka, M.; Colliex, C.; Iijima, S. *Chem. Phys. Lett.* **2000**, *316*, 365.

(34) Tuinstra, F.; Koenig, J. L. *J. Chem. Phys.* **1970**, *53*, 1126.

(35) Wilhelm, H.; Lelaurain, M.; McRae, E.; Humbert, B. *J. Appl. Phys.* **1998**, *84*, 6552.

(36) Kim, N. S.; Lee, Y. T.; Park, J.; Ryu, H.; Lee, H. J.; Choi, S. Y.; Choo, J. *J. Phys. Chem. B* **2002**, *106*, 9286.

(37) Massalski, T. B. *Binary Alloy Phase Diagrams*; American Society for Metals: Ohio, 1986.

(38) Raynor, G. V.; Rivlin, V. G. *Phase Equilibria in Iron Ternary Alloys*; Institute of Metals: London, 1988.

(39) Smithells, C. J. *Smithells' Metals Reference Book*, 7th ed.; Brandes, E. A., Brook, G. B., Eds.; Butterworth-Heinemann Ltd.: London, 1992.

(40) Baker, R. T. K. *Carbon* **1989**, *27*, 315.

(41) Bower, C.; Zhou, O.; Zhu, W.; Werder, D. J.; Jin, S. *Appl. Phys. Lett.* **2000**, *77*, 2767.

(42) Choi, Y. C.; Shin, Y. M.; Lee, Y. H.; Lee, B. S.; Park, G.-S.; Choi, W. B.; Lee, N. S.; Kim, J. M. *Appl. Phys. Lett.* **2000**, *76*, 2367.

(43) Lee, Y. T.; Park, J.; Choi, Y. S.; Ryu, H.; Lee, H. J. *J. Phys. Chem. B* **2002**, *106*, 7614.

(44) Lee, C. J.; Park, J. *J. Phys. Chem. B* **2001**, *105*, 2365.

(45) Lee, Y. T.; Kim, N. S.; Park, J.; Yang, H.; Ryu, H.; Lee, H. J. Submitted for publication to *J. Phys. Chem. B.*

(46) Terrones, M.; Ajayan, P. M.; Banhart, F.; Blase, X.; Carroll, D. L.; Charlier, J. C.; Czerw, R.; Foley, B.; Grobert, N.; Kamalakaran, R.; Kohler-Redlich, P.; Rühle, M.; Seeger, T.; Terrones, H. *Appl. Phys. A* **2002**, *74*, 355.